Title

Click-EM for imaging metabolically tagged nonprotein biomolecules.

Journal

Nature chemical biology, 12(6)

ISSN

1552-4450

Authors

Ngo, John T

Adams, Stephen R

Deerinck, Thomas J

et al.

Publication Date

2016-06-01

DOI

10.1038/nchembio.2076

Peer reviewed

HHS Public Access

Author manuscript

Nat Chem Biol. Author manuscript; available in PMC 2016 October 25.

Published in final edited form as:

Nat Chem Biol. 2016 June ; 12(6): 459–465. doi:10.1038/nchembio.2076.

Click-electron microscopy for imaging metabolically tagged non-protein biomolecules

John T. Ngo[1,8], **Stephen R. Adams**[1], **Thomas J. Deerinck**[2], **Daniela Boassa**[2], **Frances Rodriguez-Rivera**[6], **Sakina F. Palida**[1], **Carolyn R. Bertozzi**[5,7], **Mark H. Ellisman**[2,3], and **Roger Y. Tsien**[*,1,2,4,5]

[1]Department of Pharmacology, University of California, San Diego, La Jolla, CA 92093

[2]National Center for Microscopy and Imaging Research, University of California, San Diego, La Jolla, CA 92093

[3]Department of Neurosciences, University of California, San Diego, La Jolla, CA 92093

[4]Department of Chemistry & Biochemistry, University of California, San Diego, La Jolla, CA 92093

[5]Howard Hughes Medical Institute

[6]Department of Chemistry, University of California, Berkeley, CA 94720

[7]Department of Chemistry, Stanford University, Stanford, CA 94305

Abstract

Electron microscopy (EM) has long been the main technique to image cell structures with nanometer resolution, but has lagged behind light microscopy in the crucial ability to make specific molecules stand out. Here we introduce “Click-EM,” a labeling technique for correlative light microscopy and EM imaging of non-protein biomolecules. In this approach, metabolic labeling substrates containing bioorthogonal functional groups are provided to cells for incorporation into biopolymers by endogenous biosynthetic machinery. The unique chemical functionality of these analogs is exploited for selective attachment of singlet oxygen-generating fluorescent dyes via bioorthogonal “click chemistry” ligations. Illumination of dye-labeled structures generates singlet oxygen to locally catalyze the polymerization of diaminobenzidine into an osmiophilic reaction product that is readily imaged by EM. We describe the application of Click-EM in imaging metabolically tagged DNA, RNA, and lipids in cultured cells and neurons, and highlight its use in tracking peptidoglycan synthesis in the Gram-positive bacterium *Listeria monocytogenes*.

[*]To whom correspondence should be addressed: ; Email: rtsien@ucsd.edu

[8]Current Address: Department of Biomedical Engineering, Boston University, Boston, MA 02138

AUTHOR CONTRIBUTIONS

J.T.N, S.R.A, T.J.D., D.B, F.R., and S.F.P. performed experiments. J.T.N, S.R.A, T.J.D., D.B, F.R., S.F.P., C.R.B., M.H.E., and R.Y.T. analyzed data and prepared the manuscript.

COMPETING FINANCIAL INTERESTS

The authors declare no competing financial interest.

INTRODUCTION

Electron microscopy (EM) has long been the main technique to image cell structures with nanometer resolution, but has lagged behind light microscopy in the crucial ability to make specific molecules stand out. Antibodies have traditionally been used to introduce biomolecule-specific contrast to cells through direct conjugation with electron-dense secondary labels (such as gold nanoparticles); however, conventional immuno-electron microscopy (immuno-EM) is technically demanding because cells must be burdensomely cryoprotected and ultracryosectioned in order for large macromolecules to access intracellular sites. Detergent permeabilization, which facilitates antibody penetrance for immunofluorescence staining, degrades EM-visible cellular landmarks ("ultrastructure") and is therefore generally avoided during sample preparation. Replacement of gold particles with labels capable of polymerizing diaminobenzidine (DAB) enables catalytic amplification [1–2], but use of antibody conjugates of such labels still requires cryosectioning or detergent permeabilization in order to stain intracellular epitopes.

Genetically encoded EM tags that polymerize DAB can overcome these challenges because labeling occurs prior to fixation, and all auxiliary reagents required for generating contrast (O_2, DAB, OsO_4) are small molecules that readily permeate cell membranes. Tags such as miniSOG [3] and the tetracysteine motif bound to ReAsH (TC/ReAsH) [4] polymerize DAB through photogenerating singlet oxygen ($^1O_2$), a short-lived excited state of oxygen that produces a localized polymeric precipitate in the presence of DAB that can be stained with osmium and therefore readily distinguished by EM (Fig. 1a). We have previously shown that photooxidation-based polymerization of DAB occurs within nanometers of the fluorophore itself and is capable of outlining the surfaces of the labeled structure with the osmiophilic product [3–4]. DAB can also be polymerized enzymatically using a genetically encoded peroxidase-based tag such as APEX [5–6]. Together, these tags represent a versatile toolkit for imaging genetically tagged proteins by EM.

What remains missing from the EM toolkit, however, are analogous tools for imaging non-protein biomolecules, such as glycans, nucleic acids and lipids. Non-protein biomolecules comprise a significant fraction of living matter, and a simple and generalizable method for visualizing them by EM would substantially enhance our ability to dissect cellular biochemistry at the nanometer scale. While genetically encoded tags are powerful tools for imaging proteins, their direct application to other classes of biomolecules can be challenging. For instance, fusion of a fluorescent protein to the bacteriophage MS2 coat protein can be used to detect transcripts tagged with a cognate stem-loop RNA sequence, but imaging studies using such probes can be confounded by signal arising from both RNA-bound and -unbound reporter proteins [7].

Substantial progress toward fluorescence imaging of non-protein biomolecules has been made using the technology of metabolic labeling followed by bioorthogonal ligation with imaging probes. Through this approach, cell-surface glycans [8], nucleic acids [9–10], lipids [11] as well as proteins [12] have been imaged in various biological settings. These successes suggested that bioorthogonal labeling might be extended to other imaging modalities such as EM. Here we describe "Click-EM," an EM imaging technique for direct

visualization of non-protein biomolecules via DAB polymerization. In this approach, metabolic analogs containing bioorthogonal functional groups (including artificial monosaccharides, nucleotides, fatty acids, or other metabolites) are provided to cells and incorporated into biopolymers by endogenous biosynthetic machinery. The unique chemical functionality of these analogs is exploited for selective attachment of $^1O_2$-generating fluorescent dyes via bioorthogonal "click chemistry" reactions [13–17]. Dye-labeled biomolecules can be imaged by fluorescence imaging and correlated to EM observations through detection of photogenerated DAB precipitates. We describe the application of Click-EM in imaging metabolically tagged DNA, RNA, and lipids in cultured cells and neurons, and highlight its use in tracking peptidoglycan synthesis in the Gram-positive bacterium *Listeria monocytogenes*.

RESULTS

Screening of dyes for Click-EM DAB photooxidation

We sought dyes capable of efficiently photooxidizing DAB that could also be selectively conjugated to metabolically tagged biomolecules in fixed cells. In an initial screen we tested 13 azide-functionalized dyes with varying excitation wavelengths ranging from blue to far-red (Supplementary Results, Supplementary Fig. 1), including dyes that are known to photogenerate substantial levels of $^1O_2$, such as eosin [18], methylene blue [19], and IRDye700DX [20]. Eosin, a tetrabrominated derivative of fluorescein, has previously been used for DAB photooxidation as a conjugate to antibodies [2] or phalloidin [21]. The heavy atoms (bromines) on eosin increases the likelihood that the photoexcited chromophore will undergo an intersystem crossing (ISC) to the triplet state, an energy state from which $^1O_2$ can be generated from ground state O_2. Dyes that were not expected to generate significant amounts of $^1O_2$, such as AlexaFluor-647 (AF647), Cy5.5, and Sulphorhodamine-101 (SR101) were also tested. AlexaFluor-647 and Cy5.5, both of which are derived from Cy5, seemed unlikely to generate substantial levels of $^1O_2$ given that cyanines generally exhibit very low ISC quantum yields ($\Phi_{ISC} < 0.003$ for Cy5 [22]) in the absence of heavy-atom substitution [22–23]. We thought that SR101 was also unlikely to produce sufficient amounts of $^1O_2$ for DAB photooxidation given that nearly all photons absorbed by SR101 result in fluorescence emission [24].

To assess the performance of each of the selected dyes, we labeled HeLa cells with EdU (5-ethynyl-2′-deoxyuridine, Fig. 1b), an alkyne-containing thymidine analog that is incorporated into DNA during replication [9]. Following an overnight pulse with EdU, cells were fixed and subjected to Cu(I)-catalyzed azide–alkyne cycloaddition (CuAAC, a reaction referred to as "click chemistry") [13–15] with azide-functionalized derivatives of the selected dyes. Individual dyes were then tested for their ability to photooxidize DAB by immersion of labeled cells in a solution of DAB followed by intense illumination through an appropriate band pass filter. After 5 minutes of illumination, successful DAB photooxidation was judged by the appearance of optically dense precipitates that were visible under transmitted light. The photooxidation efficiency and specificity of each dye was estimated by the opacity and localization of the generated precipitates, which we expected to be predominantly nuclear due to incorporation of EdU into DNA.

Of the 13 dyes tested, 10 generated detectable DAB precipitates following 5 minutes of illumination (Supplementary Figure 2). Precipitates were not observed in cells labeled with the control dyes AF633-azide, Cy5.5-azide, and SR101-azide. Of the photooxidizing dyes, eosin-azide produced DAB precipitates of the greatest opacity, though precipitates were detected throughout entire cells, including cytosolic areas where we did not expect EdU-labeled DNA to be present. Eosin possesses a substantial $^1O_2$ quantum yield (Φ_Δ=0.57 [18]), albeit a low fluorescence quantum yield (Φ_F=0.20 [25]). Owing to the presence of four bromine atoms, eosin-azide is quite hydrophobic, and extranuclear DAB precipitation is likely due to non-specific binding of the chromophore to hydrophobic cellular components.

After eosin-azide, the second most efficient photooxidizer was dibromofluorescein-azide (DBF-azide, Fig. 1b). DBF possess a slightly decreased Φ_Δ (0.42) [18] and contains only two bromine atoms, making it less hydrophobic than eosin. Following CuAAC ligation with EdU-labeled cells, fluorescence emission from DBF-azide co-localized with Hoechst 33342 staining (Supplementary Fig. 3). Dye-labeled control cells that were not exposed to EdU did not exhibit detectable levels of DBF-azide fluorescence. Subsequent DAB photooxidation using DBF-azide produced exclusively nuclear precipitates (Fig. 1c, Supplementary Fig. 2). The nuclear specificity of DAB precipitation by DBF-azide was maintained over prolonged illumination up to 15 minutes, at which point fully opaque DAB precipitates were generated (Supplementary Fig. 4). Thus, DBF-azide is capable of efficiently photooxidizing DAB and can be conjugated to alkyne-labeled biomolecules via CuAAC with excellent specificity.

Click-EM imaging of newly EdU-labeled DNA using DBF-azide

Following photooxidation using DBF-azide, EdU-labeled cells were stained with OsO_4 (Fig. 1d), embedded in resin, and cut to 80 nm thin sections before imaging by transmission electron microscopy (TEM). On EM micrographs, osmium-stained DAB precipitates appeared as discernable contrast in patterns that correlated with DBF-azide fluorescence (Fig. 1e), and were consistent with the localization of DNA. To determine selectivity of DAB deposition at the level of EM, we compared photooxidized and non-photooxidized cells (those residing outside the area of illumination). Non-photooxidized cells displayed the expected contrast due to OsO_4 (1% w/v) staining of endogenous nuclear components (Fig. 1f). Notably, the extranuclear regions of photooxidized and non-photooxidized cells displayed similar levels of staining, indicating that little or no DAB was non-specifically precipitated during photooxidation.

We captured images of EdU-labeled cells occupying various stages of the cell cycle (Fig. 1g–m). In cells that were likely in S-phase at the time of fixation, EdU labeling was distributed throughout the nucleus, and staining was observed along the nuclear periphery, at the edges of nucleoli, and subnuclear regions where replication foci are localized during mid-S-phase [26–27] (Fig. 1g–i). Mitotic cells in prometaphase and metaphase exhibited darkly stained condensed chromosomes (Fig. 1j–k), and cells in telophase displayed staining that appeared to represent various degrees of chromatin decondensation (lightly stained extensions radiating from tightly packed and darkly stained regions, Fig. 1l–m).

A significant advantage of the photooxidation procedure is that DAB precipitates are photogenerated within intact cells, allowing electron density to be introduced at labeled sites

throughout entire cellular volumes. In contrast, immuno-EM of cell cryosections results in a sparse labeling of only a fraction of total epitopes (those accessible at the section surface). We exploited the staining uniformity afforded by DAB photooxidation to visualize EdU labeled chromosomes in 3-dimensions through stereomicroscopic analysis of individual sections (Supplementary Fig. 5). Additionally, entire volumes of EdU-labeled HEK293 cells were reconstructed using serial block face-scanning EM (SBEM), a technique in which sequential surface images are collected from a piece of mounted resin containing labeled cells of interest between rounds of automated, on-stage serial sectioning (Fig. 2, Supplementary Movie 1). Labeling of DNA in HeLa and HEK293 cells demonstrates the potential of Click-EM to visualize non-protein molecules with excellent temporal and spatial resolution.

Click-EM imaging of nascent RNAs

Next we applied Click-EM to visualize nascent transcripts using 5-ethynyl-uridine (EU, Fig. 3a), an alkyne-containing uridine analog that is selectively incorporated into RNA [10]. Three different RNA polymerase (RNAP) complexes perform nuclear RNA synthesis: RNAP I synthesizes pre-ribosomal RNAs (pre-rRNAs) and is localized to nucleoli, RNAP II is nucleoplasmic and transcribes messenger RNAs (mRNAs), and RNAP-III (also nucleoplasmic) synthesizes small RNA molecules, such as transfer RNAs (tRNAs) and the 120 nucleotide 5S-rRNA. Fluorescence imaging of EU-labeled cells revealed a predominantly nuclear localization of labeled transcripts with intensely stained nucleoli (Fig. 3b). Consistent with previous observations [10], inhibition of RNAP I by actinomycin selectively abolished nucleolar staining, confirming that nucleolar signal arose from EU incorporation by RNAP I transcriptional activity.

When imaged at the level of EM, EU-labeled transcripts were similarly distributed, though in addition to strong nucleolar staining and diffuse cytoplasmic labeling, we also detected punctate nucleoplasmic densities that were not observed by fluorescence microscopy (Fig. 3c–e). Previous studies using immunogold staining of cells labeled with 5-bromouridine-5′-triphosphate (BrUTP) or biotinylated cytidine-5′-triphosphate (biotin-14-CTP) observed clustered gold particles that co-localized with either RNAP II or RNAP III in nucleoplasmic “transcription factories” [28–29]. Additionally, labeling of nascent transcripts within transcription factories was sensitive to inhibition of the associated RNAP. Similarly, we found that inhibition of RNAP II and RNAP III using α-amanitin [30] abolished the punctate nucleoplasmic densities we observed by Click-EM (Fig. 3f–g). Thus, the nucleoplasmic densities observed by Click-EM likely represent nascent RNA molecules emerging from RNAP II and RNAP III transcription factories. This observation illustrates that Click-EM imaging of EU-labeled transcripts is in agreement with established methods of imaging newly synthesized RNAs [28].

Click-EM imaging of choline-containing phospholipids

Choline-containing phospholipids (Cho-phospholipids) play important roles in various signaling pathways and are the most abundant phospholipids found in cellular membranes. Cho-phospholipids can be tracked via fluorescence microscopy using choline analogs such as propargyl-choline [11] and azido-choline (**AzCho,** Fig. 4a) [31]. Azide-functionalized

analogs such as AzCho are especially versatile metabolic labeling substrates, since in addition to modification by CuAAC, they are also susceptible to strain-promoted ligation with cyclooctynes—a reaction referred to as “copper free click chemistry” that is compatible with live cells [16–17]. To test the applicability of copper-free click chemistry to Click-EM we reacted AzCho-labeled HeLa cells with a dibenzoazacyclooctyne (DIBAC)-functionalized [32] derivative of the far-red excited dye IRDye700DX (IRDye700DX-DIBAC, Supplementary Fig. 1). Control cells that were not exposed to AzCho exhibited only minimal levels of background fluorescence following dye-labeling (Supplementary Fig. 6), while AzCho-labeled cells revealed bright staining of intracellular membranes in patterns similar to those previously observed using bioorthogonal choline analogs [11].

DAB photooxidation using IRDye700DX-DIBAC in AzCho-labeled cells was specific and generated precipitates in patterns that correlated with dye fluorescence (Fig. 4b–c). By EM we observed continuous staining along intracellular membranes, including those of the ER, nuclear envelope, and mitochondria (Fig. 4d). Under high magnification, sites of ER:mitochondria contacts and the intricate folds of inner mitochondrial membranes were visible (Fig. 4e). In cultured cortical neurons, we observed AzCho staining on various membranes in neuronal somata, axons, dendrites, and synapses (Supplementary Fig. 7). The ER membrane was the most intensely stained structure in both cell types examined, consistent with its high composition of choline-containing phospholipids. In mammals, the ER membrane contains more choline than any other cellular membrane and is composed of nearly 60% phosphatidylcholine [33]. Mitochondrial membranes contain less choline-phospholipids than the ER membrane and were less intensely stained by comparison. To confirm that the observed EM contrast was due to osmium-stained DAB precipitates deposited during photooxidation, and not due to intrinsic osmiophilicity of these membranes, we imaged cells at the edge of the photooxidation region. In cells that partially occupied both illuminated and non-illumined areas, membrane staining was detected only in light-exposed areas (Supplementary Fig. 8), thus verifying that the observed contrast was due to light-deposited DAB precipitates.

Click-EM imaging of peptidoglycan (PG) synthesis

Finally, we applied Click-EM to image bacterial peptidoglycan, an essential cell component of most bacterial species that is also the target of many antibiotics. As previously reported in the context of fluorescence imaging, we used D-propargylglycine (henceforth abbreviated as AlkDAla, Fig. 5a, Supplementary Fig. 9) [34] to label peptidoglycan (PG) in the pathogenic Gram-positive bacterium *Listeria monocytogenes.* There are two primary routes through which D-amino acids are incorporated into *L. monocytogenes* PG: 1) periplasmic (extracellular) addition to cross-linked PG peptides, and 2) cytosolic (intracellular) incorporation into PG precursors [35–36] (Fig. 5b). Previous analyses using mass spectrometry and light microscopy suggest that AlkDAla is incorporated via the cytosolic pathway in *L. monocytogenes* [34]—however, it is difficult to selectively distinguish cytosolic AlkDAla-containing intermediates using conventional fluorescence imaging. In the cytosolic addition mechanism, D-amino acids are incorporated into a precursor that transfers a phospho-*N*-acetylmuramyl-pentapeptide moiety to undecaprenol, forming the membrane-anchored intermediate Lipid-I. Subsequent attachment of *N*-acetylglucosamine to Lipid-I

results in the formation of Lipid-II, the final cytosolic intermediate in PG biosynthesis. During cell growth, Lipid-II is transported to the extracellular face of the bacterial membrane for subsequent incorporation into the PG mesh via transglycosylation.

Direct imaging of labeled intermediates along the cytoplasmic leaflet of the plasma membrane would provide definitive proof of a cytosolic route of AlkDAla incorporation. However, distinguishing intracellular precursors from extracellular PG by light microscopy is challenging because they are separated only by the thickness of the cell membrane (approximately 7 nm in *L. monocytogenes* [37]). Because EM provides exquisite resolution, we anticipated that Click-EM would permit us to unambiguously distinguish labeled extracellular PG and its cytoplasmic intermediates. In an initial analysis, we labeled *L. monocytogenes* cells lacking PBP5 (ΔPBP5) [38], an extracellular D,D-carboxypeptidase that removes D-amino acids from PG along the length of the organism [34]. Elimination of PBP5 was used to ensure maximal incorporation of the analog into PG and its biosynthetic intermediates. Following an overnight labeling with AlkDAla, cells were fixed, subjected to CuAAC ligation with DBF-azide, and subsequently used for DAB photooxidation.

EM imaging of photooxidized cells revealed electron-dense staining along the cell perimeter (Fig. 5c). Under high magnification, two distinct bands of staining could be clearly distinguished: a thick band of extracellular PG and a thin intracellular band separated by a region of reduced contrast representing the plasma membrane (Fig. 5d, Supplementary Fig. 10a). In order to confirm the accuracy of these assignments, we labeled wild-type *L. monocytogenes* cells using a short pulse with AlkDAla (40 minutes). Previous fluorescence imaging of wild-type cells labeled under similar conditions revealed a predominantly septal and polar localization of AlkDAla, presumably due to removal of the analog along the cell length by endogenous PBP5 [34]. EM imaging revealed thick segments of staining at the poles of labeled wild-type cells, thus confirming our ability to identify extracellular PG (Fig. 6a, Supplementary Fig. 10b). We additionally detected a thin and continuous contour of staining in wild-type cells that, similar to ΔPBP5 cells, was separated from extracellular PG by the plasma membrane.

To determine whether AlkDAla is incorporated solely by the cytoplasmic mechanism, we labeled wild-type cells with AlkDAla in the presence of ramoplanin, a glycolipodepsipeptide antibiotic that inhibits the transglycosylation step of PG synthesis [39]. Ramoplanin prevents the transfer of disaccharide-pentapeptide monomers into growing PG strands by binding Lipid II extracellularly, thereby halting D-amino acid addition to PG via the cytosolic route. Thus, the absence of extracellular labeling on ramoplanin-treated cells would support a solely cytosolic route of AlkDAla incorporation, whereas extracellular detection of AlkDAla would suggest dual modes of addition. Because ramoplanin acts extracellularly, we anticipated that the drug would have no effect on cytoplasmic synthesis of PG intermediates and thus expected cells to retain intracellular staining. Consistent with this prediction, we observed intracellular staining in ramoplanin-treated cells demonstrating that ramoplanin does not prevent the incorporation of AlkDAla into cytoplasmic intermediates (Fig. 6b). Extracellular staining was not detected on ramoplanin-treated cells, thus suggesting that AlkDAla is added to *L. monocytogenes* PG exclusively through the cytosolic route and that extracellular (periplasmic) addition of the analog to cross-linked PG peptides does not occur.

DISCUSSION

As demonstrated here, the Click-EM photooxidation technique provides a simple and direct means for determining the detailed cellular distribution of metabolically tagged (non-protein) biomolecules. Click-EM is advantageous over conventional immuno-EM techniques because the biomolecules of interest are labeled prior to fixation and all auxiliary reagents required for generating contrast (click chemistry reaction components, O_2, DAB, and OsO_4) are small molecules that readily diffuse into fixed cells. Click-EM permits high quality preservation of EM-visible landmarks, the integrity of which is essential to assigning the precise location of labeled biomolecules. Application of the DAB photooxidation technique allows electron density to be deposited at labeled sites throughout entire cellular volumes, thus enabling 3-dimensional biomolecular localization via stereoscopic analysis, electron tomography, and SBEM.

Metabolic tagging using radioisotopic labels has previously been applied to image labeled biomolecules using autoradiographic EM detection [40], but these methods are tedious, rarely used, and of far lower resolution than alternative techniques [41–42]. Previously reported techniques relying on immunogold detection of incorporated metabolic labels are burdened by the limitations and challenges associated with the membrane impermeability of antibodies and the random detection of only a small fraction of total epitopes. For instance, EM imaging of propargyl-choline by attachment of biotin followed by detection using anti-biotin antibody and gold nanoparticle-conjugated protein A results in only sparse decoration of intracellular membranes [11]. In contrast, Click-EM imaging of AzCho reveals continuous staining along membrane contours (Fig. 3c), which not only aligns with fluorescence imaging of choline analogs, but also more accurately depicts the distribution and packing-density of choline-modified phospholipids in cell membranes.

We exploited the advantages of Click-EM for nanoscale interrogations of metabolically tagged DNA, RNA, and lipids in cultured mammalian cells and neurons. Additionally, we used Click-EM to track the route of AlkDAla metabolism from its initial incorporation into cytosolic Lipid-I to its eventual integration into *L. monocytogenes* PG (Figs. 5–6). The superb resolution of Click-EM enabled us to distinguish extracellular PG from its intracellular intermediates (which are separated by only 7 nm) and was essential for our analysis. Because gold nanoparticles used in immuno-EM are bulky (typically 5–25 nm in diameter) and attached to macromolecules that are also large (an immunoglobulin is ~9 nm and protein A is ~5 nm in length), individual labels can be situated many nanometers away from a labeled site. Thus, use of immunogold staining may not have provided the resolution necessary to distinguish various AlkDAla-labeled species in the bacterium.

Click-EM may be further improved through development of strategies for localizing labeled biomolecules within the context of specific proteins or genomic loci. Dual labeling of this kind may be achieved through combining Click-EM with correlative super-resolution imaging of fluorescent proteins that survive osmium staining [43], or selective targeting of fluorescent dyes that can be imaged in-resin [44]. Though we did not attempt to determine the detection sensitivity of the method, we believe Click-EM can be applied to image low abundance molecules through the catalytic amplification afforded by DAB photooxidation.

Nevertheless, the sensitivity of the method may be improved through identification of dyes with increased $^1O_2$ yields that can be specifically attached to metabolically labeled structures, or those that exhibit “turn on” behavior following ligation [45–46]. Alternatively, increasing dye-ligation yields by subjecting cells to multiple rounds of CuAAC can augment the detection of labeled biomolecules without compromising selectivity [9].

Click-EM should find widespread applications in the ultrastructural localization of many diverse classes of biomolecules. In principle, the method should be applicable to any biomolecule that can be metabolically tagged with a bioorthogonal functional group. Throughout this work, we compared photooxidized and non-photooxidized cells in order to identify DAB-specific signals on EM micrographs. In several cases, image interpretation was further aided by imaging of drug-treated cells, mutant cells, or those occupying different stages of the cell cycle. Future Click-EM users should employ similar controls to ensure that DAB-derived signals can be distinguished from ultrastructural contrast. Light-absorbing compounds (such as certain pharmacological agents, fluorescent counter stains, etc.) should be tested for potential $^1O_2$-photogenerating activity prior use. While the applications reported here were focused on non-protein biomolecules, Click-EM should also be useful for imaging discrete subpopulations of proteins, such as those that are post-translationally modified [8], or those exhibiting a specific enzymatic activity [47]. Also, Click-EM could be coupled with molecule-specific, proximity-enhanced approaches such as those recently described for labeling glycans and individual proteins [48–49]. Global incorporation of azide- or alkyne-containing noncanonical amino acids [12, 50] in combination with Click-EM may be an advantageous strategy for imaging localized neuronal protein synthesis in dendrites, a neuronal subregion that is difficult to resolve by light microscopy. Additional enticing applications for Click-EM include imaging of labeled biomolecules in other cellular subregions and structures that are difficult to fully resolve using light microscopy, such as axon terminals, mitochondria, synaptic vesicles, and autophagosomes.

ONLINE METHODS

Metabolic Labeling Reagents

EdU (5-ethynyl-2′-deoxyuridine) and EU (5-ethynyl uridine) were purchased from Life Technologies. AzCho (azido-choline) was synthesized according to previously reported procedures (Li et al. *Photochem. Photobiol.* 2014, 90, 686–695) and verified by mass spectrometry prior to use. AlkDAla (D-propargylglycine) was purchased from Acros.

Reactive Dyes

Fluorescein-azide was purchased from Lumiprobe. AlexaFluor488-azide and AlexaFluor647-azide were purchased from Life Technologies. TAMRA-azide and Sulforhodamine101-azide were purchased from Click Chemistry Tools. Cy5.5 azide was purchased from AAT Bioquest.

Synthesis of reactive dyes—*N*-Hydroxysuccinimide (NHS) esters of AlexaFluor633, methylene blue, IRDye700DX were purchased from Life Technologies, ATTO-TEC GmbH, and LI-COR respectively. Eosin isothiocyanate (ITC) was purchased from Sigma.

Synthesis of DBF—To a stirred suspension of 5(6)-carboxyfluorescein (376 mg, 1 mmol) in 80% aq. HOAc (5 ml) at room temperature, bromine (102 μL, 2 mmol) was added dropwise. The solid dissolves and after stirring overnight, the crude product is collected by filtration, washed with water, and dried *in vacuo* over P_2O_5. Yield (0.5 g, 94 %). LC-MS revealed the desired product (56% by absorbance at 254 nm) with unreacted starting material (1%) and mono (5.5%), tri (15.6%) and tetrabrominated (21.7%) products, and was used without further purification. ES-MS (*m/z*): $[M]^+$ calcd. for $C_{21}H_{10}Br_2O_7$, 534.9; found, 534.8

Synthesis of DBF-NHS—Crude 5(6)-carboxy-4′,5′-dibromofluorescein (200 mg, 0.37 mmol) was dissolved in anhydrous THF (10 ml) under N_2 and N-hydroxysuccinimide (52 mg, 0.45 mmol) was added followed by diisopropylcarbodiimide (DIPC; 59 μl, 0.38 mmol). After 4h stirring at room temperature, LC-MS indicated an incomplete reaction so an additional 25 μL of DIPC was added. After overnight, the reaction mix was evaporated, dissolved in dry DMSO (1 mL), filtered and purified by prep HPLC eluting with a gradient of 10–90% acetonitrile-water-0.05% TFA in 20 mins. The collected fractions were pooled and immediately frozen and lyophilized to give a red solid. Yield (98 mg, 42%) ES-MS (*m/z*): $[M]^+$ calcd. for $C_{25}H_{13}Br_2NO_9$, 632.9; found, 632.9

Synthesis of DBF-azide—DBF-NHS (5.1 mg, mixture of 5′- and 6′-isomers, 73% pure by HPLC with 21% hydrolyzed to DBF-carboxylic acid, 5.9 μmol) dissolved in dry DMSO (100 μl) was reacted with 3-azidopropylamine (Click Chemistry Tools; 80 μmol, 8 mg) at room temperature for 1 h. LC-MS of the reaction mixture confirmed complete reaction and it was acidified with glacial acetic acid (175 μmol, 10 μl) and the desired product separated by RP-HPLC (Luna2 C18 columns, Phenomenex) with a water-acetonitrile-0.05% TFA gradient. Fractions containing the product were lyophilized, dissolved in DMSO, and quantified by absorbance in 0.1N NaOH using an extinction coefficient of 95000 $M^{-1}cm^{-1}$ (ref P. G. Bowers, G. Porter Proc. R. Soc. Lond. A 1967 299 348–353). Yield, 67%. ^1H NMR (500 MHz, DMSO-d_6) δ ppm 1.71 (t, *J*=6.85 Hz, 4 H) 1.82 (quin, *J*=6.72 Hz, 4 H) 3.45 (t, *J*=6.72 Hz, 4 H) 6.65 (d, *J*=7.83 Hz, 1 H) 6.66 (d, *J*=7.58 Hz, 1 H) 6.77 (d, *J*=6.85 Hz, 1 H) 6.79 (d, *J*=6.85 Hz, 1 H) 7.49 (dd, *J*=7.95, 0.61 Hz, 1 H) 7.74 (t, *J*=0.98 Hz, 1 H) 8.10 (dd, *J*=8.07, 0.73 Hz, 1 H) 8.18 (dd, *J*=8.07, 1.47 Hz, 1 H) 8.26 (dd, *J*=8.07, 1.71 Hz, 1 H) 8.48 (dd, *J*=1.47, 0.73 Hz, 1 H) 8.65 (t, *J*=5.62 Hz, 1 H) 8.87 (t, *J*=5.62 Hz, 1 H) 10.98 (s, 1 H) 10.99 (s, 1 H). ^{13}C NMR (126 MHz, DMSO-d_6) δ ppm 28.14, 28.24, 36.81, 36.84, 48.44, 48.47, 82.66, 82.76, 97.48, 97.53, 110.28, 110.34, 112.69, 112.80, 126.19, 127.49, 127.66, 127.76, 136.36, 140.80, 148.49, 148.57, 152.37, 154.12, 156.79, 164.44, 164.53, 167.79, 167.89. HRMS (*m/z*): $[M]^+$ calcd. for $C_{24}H_{16}Br_2N_4O_6$, 613.9437; found, 613.9436.

General synthesis of Reactive Dyes from Dye-NHS or Dye-ITC—The dye-NHS or dye-ITC (1–5 mg) dissolved in dry DMF or DMSO was reacted with a 10 to 20-fold excess of 3-azidopropylamine at room temperature for 1 h. After neutralization with glacial HOAc, the desired product was purified by RP-HPLC (Luna2 C18 columns, Phenomenex) with a water-acetonitrile-0.05% TFA gradient except for AlexaFluor633-azide and IRDye700DX-azide that used a 0.1 M triethylammmonium acetate (pH 7.0)-acetonitrile gradient. Fractions

containing the product were lyophilized, dissolved in DMSO, and quantified by absorbance using literature or manufacturer extinction coefficients.

Eosin-azide: HRMS (*m/z*): $[M]^-$ calcd. for $C_{24}H_{15}Br_4N_5O_5S$, 800.7527; found, 800.7548.

AlexaFluor633-azide: HRMS (*m/z*): $[M]^-$ calcd. for $C_{40}H_{37}F_2N_6O_{11}S_6$, 1006.0734; found, 1006.0728.

Methylene blue-azide: HRMS (*m/z*): $[M]^+$ calcd. for $C_{21}H_{26}N_7OS^+$, 590.1277; found, 590.1265.

IRDye700DX-azide: HRMS (*m/z*): $[M]^-$ calcd. for $C_{73}H_{103}N_{15}O_{24}S_6Si_3$, 10 1849.4932; found, 1849.4942.

Synthesis of Monobromo-TAMRA-azide—Monobromo-TAMRA-azide was prepared from TAMRA carboxylic acid (Novabiochem) following the method described for dibromination of rhodamine 123 (Pai et al, *Photochem. Photobiol.* 1996, 63, 161–168). LC-MS analysis of the reaction mixture indicated 2.3% monobromo, 85.5% dibromo and 12.2% starting material. The evaporated reaction mixture was subsequently treated with 1.1 equivalents of TSTU and excess triethylamine in DMSO for 4 h. Subsequent addition of an excess of 3-azidopropylamine gave the desired product which was isolated by RP-HPLC. HRMS (*m/z*): $[M]^+$ calcd. for $C_{28}H_{28}BrN_6O_4$, 590.1277; found, 590.1265.

Synthesis of Monobromo-Cy5-azide—1-(5′-carboxypentynyl)-2,3,3-trimethylindoleninium-5-sulfonate (70 mg, 0.2 mmol) (Mujumdar et al. *Bioconj. Chem.* 1994, 4, 105–111), bromomalonaldehyde dianil bromide (38.2 mg 0.1 mmol) (EP1223197A2) and anhydrous KOAc (40mg, 0.4 mmol) were refluxed in EtOH (0.5 ml) for 30 min. The reaction mix was cooled, stood overnight and crude product collected by filtration as an iridescent blue solid (62 mg). Further purification of 30 mg by RP-HPLC gave 9.5 mg of pure monobromo-Cy5-bis-carboxylic acid. Yield, 24%. ES-MS (*m/z*): $[M]^+$ calcd. for $C_{37}H_{46}BrN_2O_{10}S_2^+$, 821.2; found, 821.2. The mono NHS and azide were made by reaction of this product (5.9 mg, 7.1 μmol) with TSTU (2.2 mg, 7.1 μmol) in dry DMF (200 μl) and pyridine (20 μl) overnight. LC-MS revealed a mixture of mono- (32%) and di-NHS (4%) esters with unreacted starting material (64%). Excess 3-azidopropylamine (10 μl) was added and after 30 min, the reaction was quenched with HOAc (10 μl) to give the desired product (1.2 mg, 19%) following purification by RP-HPLC. HRMS (*m/z*): $[M]^+$ calcd. for $C_{40}H_{52}BrN_6O_9S_2^+$, 902.2342; found, 902.2338.

Synthesis of IRDye700DX-DIBAC—Prepared from the Dye-NHS by reaction with excess DBCO-amine (Click Chemistry Tools) in DMF followed by purification by RP-HPLC using a 0.1M triethylammmonium acetate pH 7.0-acetonitrile gradient. HRMS (*m/z*): $[M]^-$ calcd. for $C_{88}H_{111}N_{13}O_{25}S_6Si_3$, 2025.5446; found, 2025.5441.

Metabolic Labeling of Mammalian Cells and Neurons

Mammalian cells and neurons were maintained at 37 °C in a humidified cell culture incubator with 5% CO_2. Authenticated HEK293 and HeLa cell lines (both American Type

Culture Collection) cells were purchased directly from the vendor and the lines were morphologically correct. HeLa and HEK293 cells were cultured in imaging dishes containing poly-D-lysine coated coverslip glass bottoms (P35GC-0-14-C, MatTek Corporation) in DMEM supplemented with 10% FBS, 20 U/mL penicillin and 50 μg/mL streptomycin. Cortical neurons were dissociated by papain from postnatal day 2 (P2) Sprague Dawley rats and cultured in imaging dishes containing poly-D-lysine coated coverslip glass bottoms (P35GC-0-14-C, MatTek Corporation) in Neurobasal A medium supplemented with 1X B27 Supplements (both from Life Technologies), 2 mM GlutaMAX (Life Technologies), 20 U/mL penicillin and 50 μg/mL streptomycin. All animal procedures were approved by the Institutional Animal Care and Use Committee of UC San Diego.

EdU labeling—HeLa and HEK293 cells were labeled with EdU overnight by addition to of the analog to culture media at a final concentration of 10 μM.

EU labeling—HeLa cells were labeled with EU for 2.5 h by addition of the analog to culture media at a final concentration of 2 mM. To inhibit RNAP I activity, actinomycin-D was added to culture media (at a final concentration of 100 nM) 30 min prior to the addition of EU. To inhibit RNAP II and RNAP III, α-amanitin was added to culture media (at a final concentration of 25 μg ml^{-1}) 30 min prior to the addition of EU.

AzCho labeling—HeLa cells were labeled with AzCho overnight by addition of the analog to culture media at a final concentration of 75 μM. DIV 15 – 20 cortical neurons isolated from rats were labeled with AzCho under the same conditions.

Metabolic Labeling of *L. monocytogenes* Cells

Wild-type *L. monocytogenes* EGD-e cells were grown in Brain Heart Infusion (BHI) medium at 37 °C with shaking and labeled for 40 min or overnight. ΔPBP5 *L. monocytogenes* cells (*lmo2754::tn)* were labeled at a final concentration of 5 mM alkDala under the same growth conditions. For ramoplanin inhibition studies, cells were grown in the presence of both 1 ug/mL ramoplanin and 5 mM alkDala for 40 min. Following labeling experiments, liquid cultures were washed twice with BHI media to remove excess alkDala and prepared as glycerol stocks to be stored at −80 °C until processed for electron microscopy. Cells were thawed, rinsed once in PBS and resuspended in fresh PBS before adsorption onto poly-D-lysine coated glass-bottom imaging dishes by pipetting cultures directly on the glass surface. After 30 min at room temperature, excess liquid culture was removed and the dishes were rinsed once with fresh PBS prior to fixation and further processing as described below.

Cell Fixation

Cells were rinsed once with PBS and subsequently fixed using 2.5% (w/v) glutaraldehyde (Electron Microscopy Sciences) in a solution of 0.1 M sodium cacodylate buffer, pH 7.4 (Ted Pella Incorporated) containing 1 mM $CaCl_2$. Cell fixation was allowed to proceed for 5 min at 37 °C and then on ice for 1 h. The fixative was then removed and cells were rinsed with ice-cold cacodylate buffer (3×3 min) followed rinsing with an ice-cold solution of PBS

containing 2% BSA (w/v) (2×3 min). Cells were kept on ice in cold PBS/BSA solution while dye reaction mixtures (described below) were prepared at room temperature.

CuAAC Ligation Reactions

All dyes were stored as concentrated stocks in DMSO and diluted into reaction mixtures before use. For conjugation of azide-functionalized dyes to alkyne-labeled biomolecules (EdU, EU, and AlkDAla) we used the Click-iT Cell Reaction Buffer Kit (Life Technologies) according to the manufacturer's protocol with the following modifications: 1) Cells were fixed with 2.5% (w/v) glutaraldehyde as described in the preceding section, 2) cells were not subjected to permeabilization with TritonX-100 or another detergent, 3) the azide-functionalized dyes described in the "Reactive Dyes" section above were used at concentrations between 5–10 μM, and 4) the "Click-iT cell buffer additive (Component C)" was replaced by a 20 mg/ml solution of sodium ascorbate in ddH_2O (prepared fresh each time immediately before use). The sodium ascorbate solution was added as the last component of the reaction cocktails by dilution (ten-fold, v/v) into reaction mixtures.

To initiate the CuACC reaction, the PBS/BSA solution was removed from the imaging dishes and immediately replaced with complete (ascorbate-containing) dye-reaction mixture. Dishes were then gently and briefly swirled before allowing reactions to proceed without further agitation for 30 min at room temperature protected from light. For the EdU-labeled cells shown in Supplementary Figs. 4 and 6, and all EU-labeled cells (Fig. 3), a total of two rounds of CuAAC reactions (using fresh reaction components) were applied in succession. Following the reaction, cells were placed on ice and rinsed with ice-cold PBS/BSA solution (3×3 min), followed by rinsing with ice-cold cacodylate buffer (2×3 min) before proceeding to the blocking step.

Copper-Free Click Chemistry Reactions

Prior to exposure of cells to IRDye700DX-DIBAC, free thiols were alkylated by treatment of fixed cells with a solution of N-ethylmaleimide (NEM, 100 mM in PBS) for 45 min at room temperature. Cells were rinsed once in PBS/BSA solution before adding a 4.4 μM solution of IRDye700DX-DIBAC in PBS (dye was diluted from a 220 uM stock in DMSO). Reactions were allowed to proceed protected from light for 30 m at room temperature. Following the reaction, cells were rinsed with ice-cold PBS/BSA solution (3×3 min), followed by rinsing with ice-cold cacodylate buffer (2×3 min) before proceeding to the blocking step.

Blocking Step

To prevent background precipitation of DAB by endogenous cellular components, cells were treated for 30 min on ice in a solution of 0.1 M sodium cacodylate buffer (pH 7.4) containing 50 mM glycine, 10 mM KCN, 5 mM aminotriazole, and 1 ul of 30% H_2O_2 per 30 mL of blocking solution.

Confocal Fluorescence Imaging and Photooxidation

Cells were imaged/photooxidized using an inverted confocal microscope outfitted with a stage chilled to 4 °C. Confocal fluorescence and transmitted light images were taken with

minimum exposure to identify transfected cells for correlative light microscopic imaging. For photooxidation, DAB (3-3′-diaminobenzidine, Sigma-Aldrich) was dissolved in 0.1 N HCl at a concentration of 5.4 mg ml^{-1} and subsequently diluted ten-fold (v/v) into sodium cacodylate buffer, pH 7.4 (with a final buffer concentration of 0.1 M), mixed, and passed through a 0.22 μm syringe filter. DAB solutions were freshly prepared on the day of photooxidation and placed on ice and protected from light before being added to the cells. Regions of interest were identified by fluorescence and images were recorded with care to avoid photobleaching. For photooxidation, samples were illuminated through an appropriate band pass filter (as indicated for each dye in Supplementary Fig. 2b) with intense light from a 150 W xenon lamp. In our initial screen of potential Click-EM dyes we used a fixed illumination period of 5 min. Samples processed for EM analysis were illuminated for 5 – 10 min, depending on the initial fluorescence intensity, the brightness of the illumination, and the optics used.

Staining of Cells for TEM and Imaging

Multiple areas on a single dish were photooxidized as described in the preceding section. Subsequently, cells were placed on a bed of ice and washed using ice-cold cacodylate buffer (5×2 min) to remove unpolymerized DAB. After washing, cell were post-fixed with 1% osmium tetroxide (Electron Microscopy Sciences) in 0.1 M sodium cacodylate buffer for 30 min on ice, then washed with ice-cold cacodylate buffer (3×2 min) and rinsed once in ice-cold distilled water. The samples were then dehydrated with an ice-cold graded ethanol series (20% (v/v), 50% (v/v), 70% (v/v), 90% (v/v), 100% (anhydrous), and 100% (anhydrous) for 3 min each) and washed once in room temperature 100% (anhydrous) ethanol for 3 min. Samples were then infiltrated with Durcupan ACM resin (Electron Microscopy Sciences, prepared according to the manufacturer's protocol) using a 1:1 solution of anhydrous ethanol:resin for 30 min on a platform with gentle rocking, then with 100% resin overnight with rocking. The next day, the resin was removed from dishes (by decanting and gentle scraping with care to avoid touching cells), replaced with freshly prepared 100% resin (3×30 min with rocking), and polymerized in a vacuum oven at 60°C for 48 hours. Subsequently, photooxidized areas of interest were identified using a dissecting microscope, sawed out using a jeweler's saw, and mounted on dummy acrylic blocks with cyanoacrylic adhesive. The coverslip was carefully removed and ultrathin sections (80 nm thick) were cut using an ultramicrotome. Electron micrographs were recorded using a JEOL 1200 EX transmission electron microscope operating at 60 kV.

Preparation of Staining Solutions for SBEM Analysis

The following solutions were prepared on Day 1 of the staining procedure immediately before use:

1. *Solution A:* a solution containing 3% (w/v) potassium ferrocyanide and 6mM $CaCl_2$ in 0.2 M cacodylate buffer was freshly prepared and mixed (1:1, v/v) with a 4% (w/v) aqueous solution of osmium tetroxide (Electron Microscopy Sciences). This solution was chilled on ice before use.

2 *Solution B:* a fresh solutions of thiocarbohydrazide was prepared (while cells were incubating Solution A, see details below) by adding 100 mg of thiocarbohydrazide (Ted Pella) to 10 ml of ddH_2O. The solution was then heated in a 60 °C oven for 30 minutes with gentle agitation/swirling every 10 min to ensure dissolution of the material.

3 *Solution C:* a 2% (w/v) osmium tetroxide was prepared by mixing equal volumes of ddH_2O and a 4% (w/v) aqueous solution of osmium tetroxide.

4 *Solution D:* a 2% uranyl acetate (w/v) was prepared by dissolution in ddH_2O.

The following solutions were prepared on Day 2 of the staining procedure immediately before use:

5 *Solution E:* 0.998 g of L-aspartic acid (Sigma-Aldrich) was dissolved in 250 ml of ddH_2O

6 *Solution F:* 0.066 gm of lead nitrate was dissolved in 10 ml of Solution E and the solution pH was adjusted to 5.5 by adding 1 N KOH dropwise. The solution was then heated in a 60° C oven for 30 minutes until completely dissolved.

Staining of Cells for SBEM and Imaging

Multiple areas on a single dish were photooxidized as described in the preceding section. Subsequently, unpolymerized DAB was removed from cells by rinsing cells with ice-cold cacodylate buffer (5×2 min) on a bed of ice. Cells were then incubated in Solution A on ice for 30 m while Solution B was prepared. At the end of the 30 min incubation, Solution A was removed and cells were rinsed (5×2 min) in ddH_2O at room temperature and subsequently incubated in Solution B at room temperature. After 10 m, Solution B was removed and cells were rinsed (5×2 min) using ddH_2O at room temperature and subsequently incubated in Solution C. After 10 min, Solution C was removed and cells were rinsed (5×2 min) using ddH_2O at room temperature and subsequently incubated with Solution D overnight in a refrigerator kept at ~4° C.

The following day cells were rinsed (5×2 min) using ddH_2O at room temperature before *en bloc* Walton's lead aspartate staining was performed by incubating cells in warm Solution F for in a 60° C oven. After 10 min, cells were removed from the oven and rinsed (5×2 min) using ddH_2O at room temperature. The cells were then subjected to dehydration using a series of ice-cold ethanol solution in water for 3 min each on a bed of ice in the following order: 20% (v/v), 50% (v/v), 70% (v/v), 90% (v/v). Subsequently, the cells were further dehydrated using two washes in ice-cold 100% (anhydrous) ethanol for 3 min each, then removed from the bed of ice and washed once in room temperature 100% (anhydrous) ethanol for 3 min. Samples were then infiltrated with Durcupan ACM resin (Electron Microscopy Sciences, prepared according to the manufacturer's protocol) using a 1:1 solution of anhydrous ethanol:resin for 30 min on a platform with gentle rocking, then with

100% resin overnight with rocking. The next day, the resin was removed from dishes (by decanting and gentle scraping with care to avoid touching cells), and replaced with freshly prepared 100% resin (3×30 min with rocking). Cells were then submerged using a small amount of resin and covered with a square piece of aclar to great a flat surface. The resin was allowed to polymerize in a vacuum oven at 60°C for 48 hours. Finally, photooxidized areas of interest were identified, sawed out using a jeweler's saw, and mounted for SBEM imaging using a Gatan 3View system (Gatan Inc.) incorporated into a Zeiss Merlin Compact SEM (Zeiss) and images recorded using 60 nm cutting intervals.

Supplementary Material

Refer to Web version on PubMed Central for supplementary material.

Acknowledgments

We gratefully acknowledge S. Phan for assistance with SBEM image processing, C. Woodford for assistance with NMR, L. Gross for assistance with mass spectrometry, and C. Hill for providing wild-type and lmo2754::tn EGD-e *L. monocytogenes*. Funding for this work was provided by NIH GM086197 (to R.Y.T. and M.H.E.), NIH GM059907 (to C.R.B), and NIH AI051622 (to C.R.B.). The work described herein was carried out using shared research resources at the National Center for Microscopy and Imaging Research (NCMIR) at UCSD supported by the NIH under award number P41 GM103412 (to M.H.E). F.R. was supported by a Ford Foundation Predoctoral Fellowship and a Chancellor's fellowship from UC Berkeley. C.R.B and R.Y.T. are Investigators in the Howard Hughes Medical Institute.

References

1. Stirling JW. Immuno- and Affinity Probes for Electron Microscopy: A Review of Labeling and Preparation Techniques. J Histochem Cytochem. 1990; 48:147–157.
2. Deernick TJ, et al. Fluorescence photooxidation with eosin: a method for high resolution immunolocalization and in situ hybridization detection for light and electron microscopy. J Cell Biol. 1994; 126:901–910. [PubMed: 7519623]
3. Shu X, et al. A Genetically Encoded Tag for Correlated Light and Electron Microscopy of Intact Cells, Tissues, and Organisms. PLoS Biology. 2011; 9:e1001041. [PubMed: 21483721]
4. Gaietta G, et al. Multicolor and electron microscopic imaging of connexin trafficking. Science. 2002; 296:503–507. [PubMed: 11964472]
5. Martell JD, et al. Engineered ascorbate peroxidase as a genetically encoded reporter for electron microscopy. Nat Biotechnol. 2012; 20:1143–1148. [PubMed: 23086203]
6. Lam SS, et al. Directed evolution of APEX2 for electron microscopy and proximity labeling. Nat Methods. 2015; 12:51–54. [PubMed: 25419960]
7. Tyagi S. Imaging intracellular RNA distribution and dynamics in living cells. Nat Methods. 2009; 6:331–338. [PubMed: 19404252]
8. Laughlin ST, Baskin JM, Amacher SL, Bertozzi CR. In vivo imaging of membrane-associated glycans in developing zebrafish. Science. 2008; 320:664–667. [PubMed: 18451302]
9. Salic A, Mitchison TJ. A chemical method for fast and sensitive detection of DNA synthesis in vivo. Proc Natl Acad Sci USA. 2008; 105:2415–2420. [PubMed: 18272492]
10. Jao CY, Salic A. Exploring RNA transcription and turnover in vivo by using click chemistry. Proc Natl Acad Sci USA. 2008; 105:15779–15784. [PubMed: 18840688]
11. Jao CY, Roth M, Welti R, Salic A. Metabolic labeling and direct imaging of choline phospholipids in vivo. Proc Natl Acad Sci USA. 2009; 106:15332–15337. [PubMed: 19706413]
12. Ngo JT, Tirrell DA. Noncanonical amino acids in the interrogation of cellular protein synthesis. Acc Chem Res. 2011; 44:677–685. [PubMed: 21815659]

13. Rostovtsev VV, Green LG, Fokin VV, Sharpless KB. A Stepwise Huisgen Cycloaddition Process: Copper(I)-Catalyzed Regioselective "Ligation" of Azides and Terminal Alkynes. Angew Chem Int Ed Engl. 2002; 41:2596–2599. [PubMed: 12203546]
14. Tornøe CW, Christensen C, Meldal M. Peptidotriazoles on solid phase: [1,2,3]-triazoles by regiospecific copper(i)-catalyzed 1,3-dipolar cycloadditions of terminal alkynes to azides. J Org Chem. 2002; 67:3057–3064. [PubMed: 11975567]
15. Wang Q, et al. Bioconjugation by copper (I)-catalyzed azide-alkyne [3+ 2] cycloaddition. J Am Chem Soc. 2003; 125:3192–3193. [PubMed: 12630856]
16. Agard NJ, Prescher JA, Bertozzi CR. A strain-promoted [3+ 2] azide-alkyne cycloaddition for covalent modification of biomolecules in living systems. J Am Chem Soc. 2004; 126:15046–15047. [PubMed: 15547999]
17. Jewett JC, Bertozzi CR. Cu-free click cycloaddition reactions in chemical biology. Chem Soc Rev. 2010; 39:1272–1279. [PubMed: 20349533]
18. Gandin E, Lion Y, Van de Vorst A. Quantum yield of singlet oxygen production by xanthene derivatives. Photochem Photobiol. 1983; 37:217–278.
19. Usui Y. Determination of quantum yield of singlet oxygen formation by photosensitization. Chem Lett. 1973; 7:743–744.
20. Kishimoto S, et al. Evaluation of oxygen dependence on in vitro and in vivo cytotoxicity of photoimmunotherapy using IR-700-antibody conjugates. Free Radic Biol Med. 2015; 85:24–32. [PubMed: 25862414]
21. Capani F, Deerinck TJ, Ellisman MH, Bushong E, Bobik M, Martone ME. Phalloidin-eosin followed by photo-oxidation: a novel method for localizing F-actin at the light and electron microscopic levels. J Histochem Cytochem. 2001; 49:1351–1361. [PubMed: 11668188]
22. Chibisov AK, Zakharova GV, Görner H. Effects of substituents in the polymethine chain on the photoprocesses in indodicarbocyanine dyes. J Chem Soc Faraday Trans. 1996; 92:4917–4925.
23. Görner H, Chibisov AK. Photoprocesses in Polymethine Dyes: Cyanines and Spiropyrane-Derived Merocyanines. CRC Handbook of Organic Photochem and Photobiol. 2004:36.1–36.21.
24. Velapoldi RA, Tønnesen HH. Corrected Emission Spectra and Quantum Yields for a Series of Fluorescent Compounds in the Visible Spectral Region. J Fluoresc. 2004; 14:465–427. [PubMed: 15617389]
25. Fleming GR, Knight AWE, Morris JM, Morrison RJS, Robinson GW. Picosecond fluorescence studies of xanthene dyes. J Am Chem Soc. 1977; 99:4306–4311.
26. Dimitrova DS, Berezney R. The spatio-temporal organization of DNA replication sites is identical in primary, immortalized and transformed mammalian cells. J Cell Sci. 2002; 115:4037–4051. [PubMed: 12356909]
27. Chagin VO, Stear JH, Cardoso MC. Organization of DNA replication. Cold Spring Harb Perspect Biol. 2010; 2:a000737. [PubMed: 20452942]
28. Iborra FJ, Pombo A, Jackson DA, Cook PR. Active RNA polymerases are localized within discrete transcription 'factories' in human nuclei. J Cell Sci. 1996; 109:1427–1436. [PubMed: 8799830]
29. Papantonis A, Cook PR. Transcription Factories: Genome Organism and Gene Regulation. Chem Rev. 2013; 113:8683–8705. [PubMed: 23597155]
30. Bensaude O. inhibiting eukaryotic transcription: Which compound to choose? How to evaluate its activity? Transcription. 2011; 2:103–108. [PubMed: 21922053]
31. Li C, Key JA, Jia F, Dandapat A, Hur S, Cairo CW. Practical labeling methodology for choline-derived lipids and applications in live cell fluorescence imaging. Photochem Photobiol. 2014; 90:686–695. [PubMed: 24383866]
32. Debets MF, et al. Aza-dibenzocyclooctynes for fast and efficient enzyme PEGylation via copper-free (3+2) cycloaddition. Chem Commun. 2009; 46:97–99.
33. van Meer G, Voelker DR, Feigenson GW. Membrane lipids: where they are and how they behave. Nat Rev Mol Cell Bio. 2008; 9:112–124. [PubMed: 18216768]
34. Siegrist MS, et al. D-Amino Acid Chemical Reporters Reveal Peptidoglycan Dynamics of an Intracellular Pathogen. ACS Chem Biol. 2013; 8:500–505. [PubMed: 23240806]

35. Cava F, de Pedro MA, Lam H, Davis BM, Waldor MK. Distinct pathways for modification of the bacterial cell wall by non-canonical D-amino acids. EMBO J. 2011; 30:3442–3453. [PubMed: 21792174]
36. Siegrist MS, Swarts BM, Fox DM, Lim SA, Bertozzi CR. Illumination of growth, division and secretion by metabolic labeling of the bacterial cell surface. FEMS Microbiol Rev. 2015; 39:184–202. [PubMed: 25725012]
37. Pittman JR, et al. Effect of Stressors on the Viability of Listeria During an in vitro Cold-Smoking Process. Agric Food Anal Bacteriol. 2012; 2:195–298.
38. Korsak D, Waldemar V, Zdzislaw M. Listeria monocytogenes EGD lacking penicillin-binding protein 5 (PBP5) produces a thicker cell wall. FEBS Micobiol Lett. 2005; 251:281–288.
39. Fang X, et al. The mechanism of action of ramoplanin and enduracidin. Mol Biosyst. 2006; 2:69–76. [PubMed: 16880924]
40. Littau VC, Allfrey VG, Frenster JH, Mirsky AE. Active and inactive regions of nuclear chromatin as revealed by electron microscope autoradiography. Proc Natl Acad Sci USA. 1964; 52:93–100. [PubMed: 14192663]
41. Gupta BL, Moreton RB, Cooper NC. Reconsideration of the resolution in EM autoradiography using a biological line source. J Microsc. 1973; 99:1–25.
42. Iborra FJ, Cook PR. The Size of Sites Containing SR Proteins in Human Nuclei: Problems Associated with Characterizing Small Structures by Immunogold Labeling. J Histochem Cytochem. 1998; 46:985–992. [PubMed: 9705963]
43. Paez-Segala MG, et al. Fixation-resistant photoactivatable fluorescent proteins for CLEM. Nat Methods. 2015; 12:215–218. [PubMed: 25581799]
44. Perkovic M, et al. Correlative Light- and Electron Microscopy with chemical tags. J Struct Biol. 2014; 186:205–213. [PubMed: 24698954]
45. Devaraj NK, et al. Bioorthogonal Turn-On Probes for Imaging Small Molecules inside Living Cells. Angew Chem Int Ed Engl. 2010; 49:2869–2872. [PubMed: 20306505]
46. Shieh P, et al. CalFluors: A Universal Motif for Fluorogenic Azide Probes across the Visible Spectrum. J Am Chem Soc. 2015; 137:7145–7151. [PubMed: 25902190]
47. Sanman LE, Bogyo M. Activity-based profiling of protease. Annu Rev Biochem. 2014; 83:249–273. [PubMed: 24905783]
48. tom Dieck S, et al. Direct visualization of newly synthesized target proteins in situ. Nat Methods. 2015; 12:411–414. [PubMed: 25775042]
49. Robinson PV, de Almeida-Escobedo G, de Groot AE, McKechnie JL, Bertozzi CR. Live-Cell Labeling of Specific Protein Glycoforms by Proximity-Enhanced Bioorthogonal Ligation. J Am Chem Soc. 2015; 137:10452–10455. [PubMed: 26280358]
50. Dieterich DC, et al. In situ visualization and dynamics of newly synthesized proteins in rat hippocampal neurons. Nat Neurosci. 2010; 13:897–905. [PubMed: 20543841]

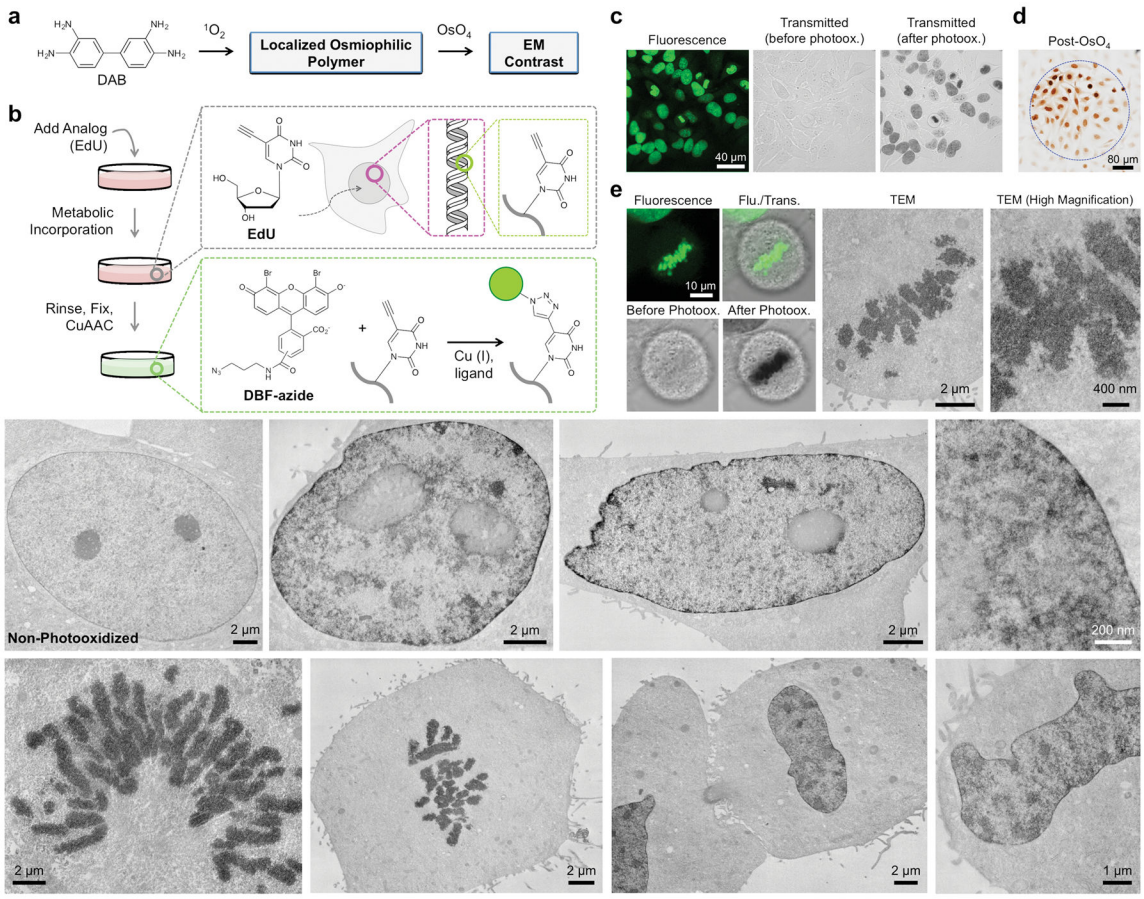

Figure 1. Click-EM imaging of EdU-labeled HeLa cells

(**a**) Schematic depicting how $^1O_2$ is used to generate EM contrast. (**b**) Schematic depicting the metabolic labeling and CuAAC reaction steps of the Click-EM procedure. Structures of EdU, DBF-azide, and their CuAAC ligation product are shown. (**c**) Fluorescence and transmitted light images of EdU-labeled HeLa cells following CuAAC ligation with DBF-azide. Transmitted light images before (middle) and after (right) photooxidation are shown; polymeric DAB precipitates accumulated during the illumination period appear as optically dense deposits that overlay with DBF-azide emission. (**d**) Photooxidized cells following osmium staining. Osmium stained DAB precipitates appear brown under white light. The dotted blue line defines the area of illumination. (**e**) Correlated light and EM images of a mitotic cell labeled with EdU and DBF-azide. The set of four images on the left were obtained by light microscopy and correspond to the same cell shown the middle and right images, which were obtained by EM. (**f–m**) EM images of EdU labeled HeLa cells: (**f**) a non-photooxidized cell, (**g–i**) S- or G2-phase cells, (**j–m**) mitotic cells.

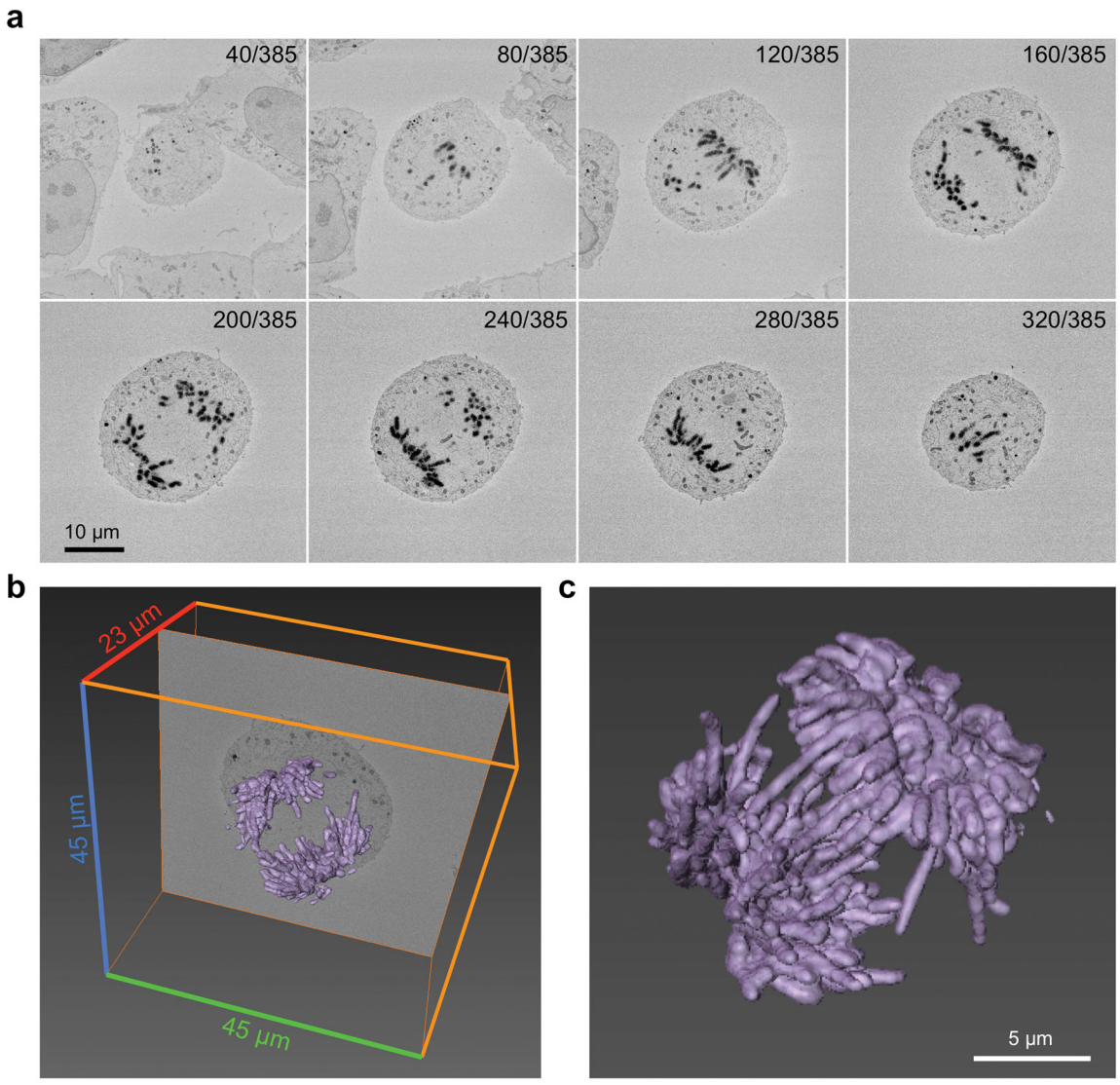

Figure 2. SBEM imaging of EdU-labeled HEK293 cells

(**a**) Montage of selected 2-dimensional (45μm × 45μm) images collected by SBEM. (**b**) A sum of 385 individual images from the area shown in (a) were used to reconstruct the full 3-dimesional volume of an EdU-labeled mitotic cell. Images were collected serially along the z-axis at 60 nm intervals (z-dimension distance = 23 μm). Signal intensity arising from EdU-labeled DNA is shown in purple. (**c**) A three-dimensional rendering of the signal arising from OsO_4-stained DAB deposits.

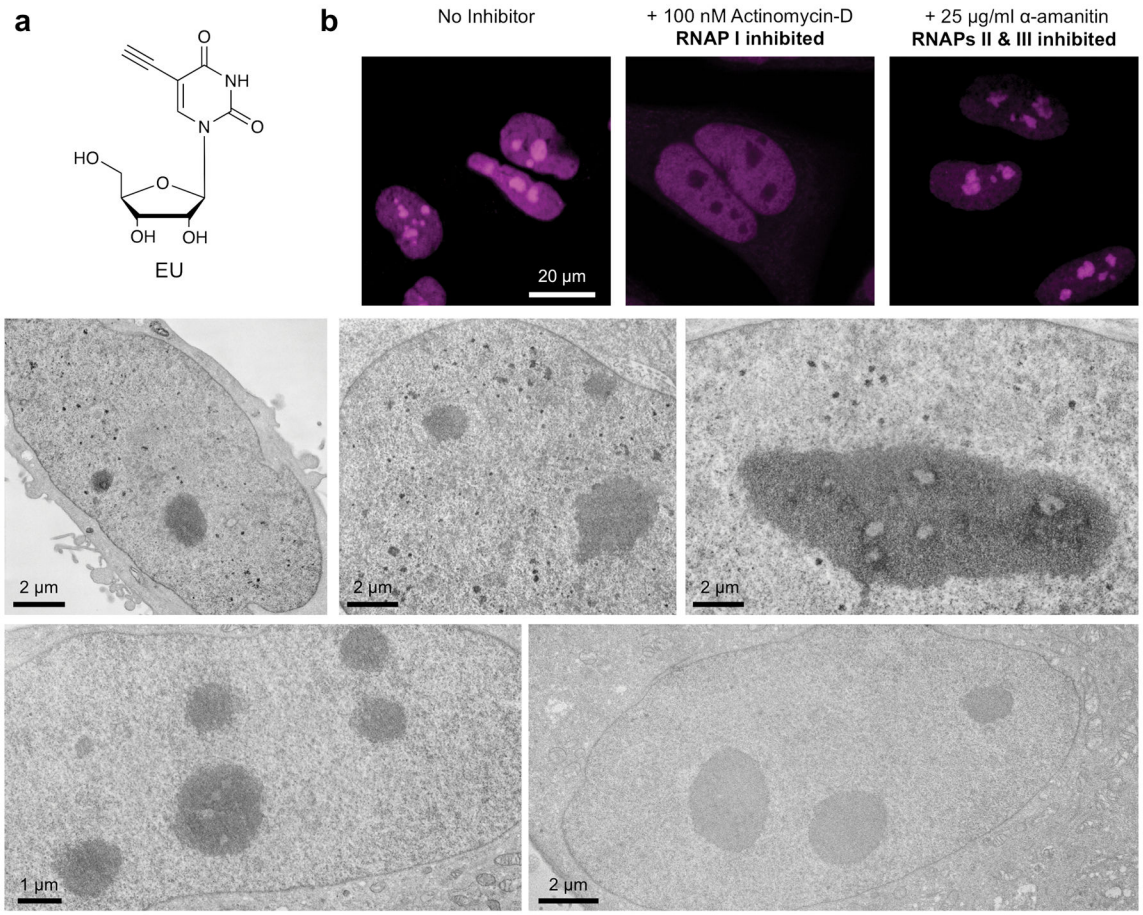

Figure 3. Imaging of nascent transcripts using EU

a) Structure of EU. (**b**) Fluorescence detection of EU-labeled transcripts in HeLa cells following CuAAC ligation with DBF-azide. (**c–g**) EM micrographs of EU labeled cells: (**c–e**) uninhibited HeLa cells exhibiting darkly stained nucleoli, diffuse nucleoplasmic labeling, and stained nucleoplasmic intensities; (**f**) the nucleus of a HeLa pulsed with EU in the presence of α-amanitin (for inhibition of RNAP II and III) exhibiting darkly stained nucleoli, but without stained nucleoplasmic intensities; (**g**) the nucleus of a non-photooxidized cell.

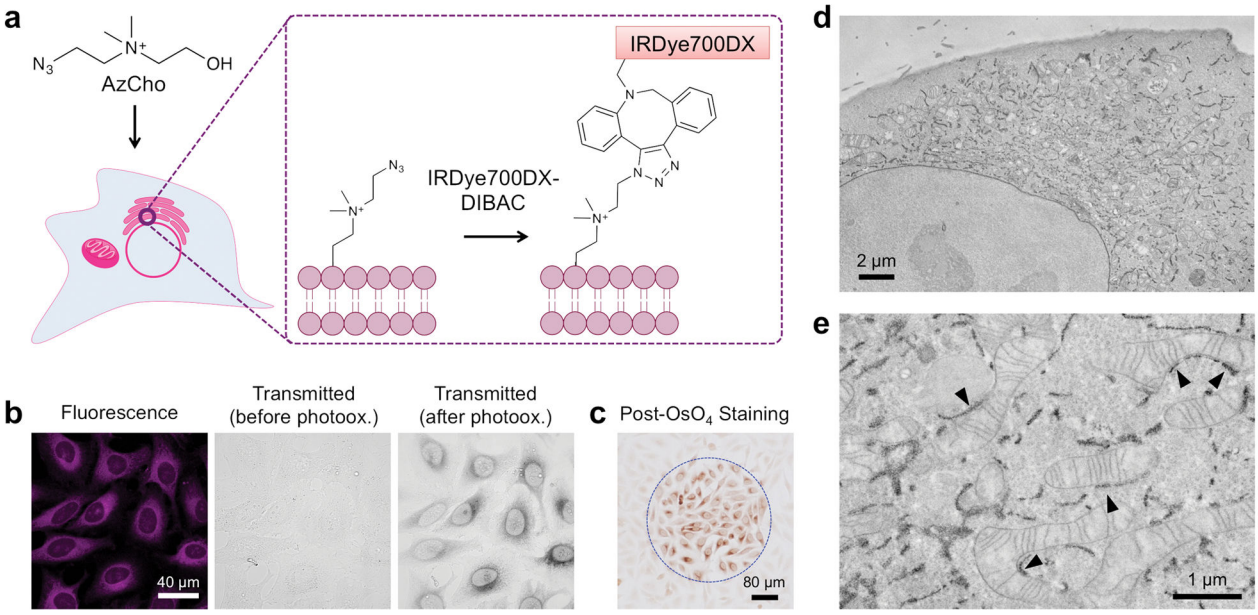

Figure 4. Click-EM imaging of AzCho labeled HeLa cells

(**a**) Schematic depicting the metabolic incorporation of AzCho into cho-phospholipids and subsequent detection of labeled membranes using copper-free click chemistry. (**b**) AzCho-labeled HeLa cells imaged by fluorescence (left) and transmitted light imaged before (middle) and after (right) DAB photooxidation. (**c**) AzCho-labeled HeLa cells imaged by white light following DAB photooxidation and OsO_4 staining. The blue dotted line indicates the area of illumination. (**d**) TEM micrograph of an AzCho labeled HeLa cell following DAB photooxidation and osmium staining. (**e**) A high magnification TEM image showing the detailed features of AzCho-labeled mitochondria, including sites of ER:mitochondria contacts (black arrowheads).

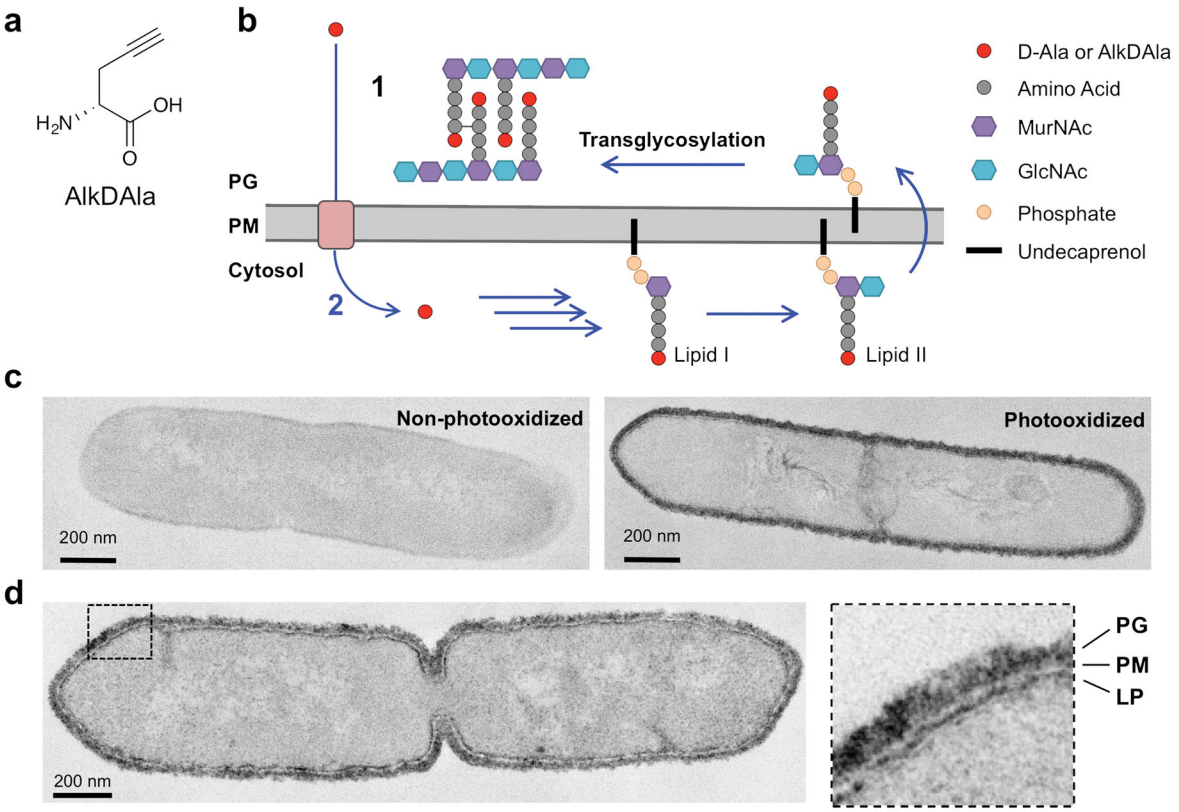

Figure 5. Click-EM imaging of PG in *L. monocytogenes*

(**a**) Structure of AlkDAla. (**b**) Schematic depicting extracellular (black arrows) and intracellular (blue arrows) routes of D-amino acid incorporation into *L. monocytogenes* PG. (**c**) TEM of images of AlkDAla-labeled *L. monocytogenes* cells. A non-photooxidized control cell (left) is shown beside a photooxidized cell (right) for comparison. (**d**) High magnification TEM of a photooxidized dividing ΔPBP5 mutant cell showing labeled extracellular PG as a thick and continuous outline of contrast. Stained intracellular precursors (IP) are depicted as a continuous contour on the cytoplasmic side of the plasma membrane (PM). The PM is embedded between stained extracellular and intracellular bands and appears as region of decreased contrast.

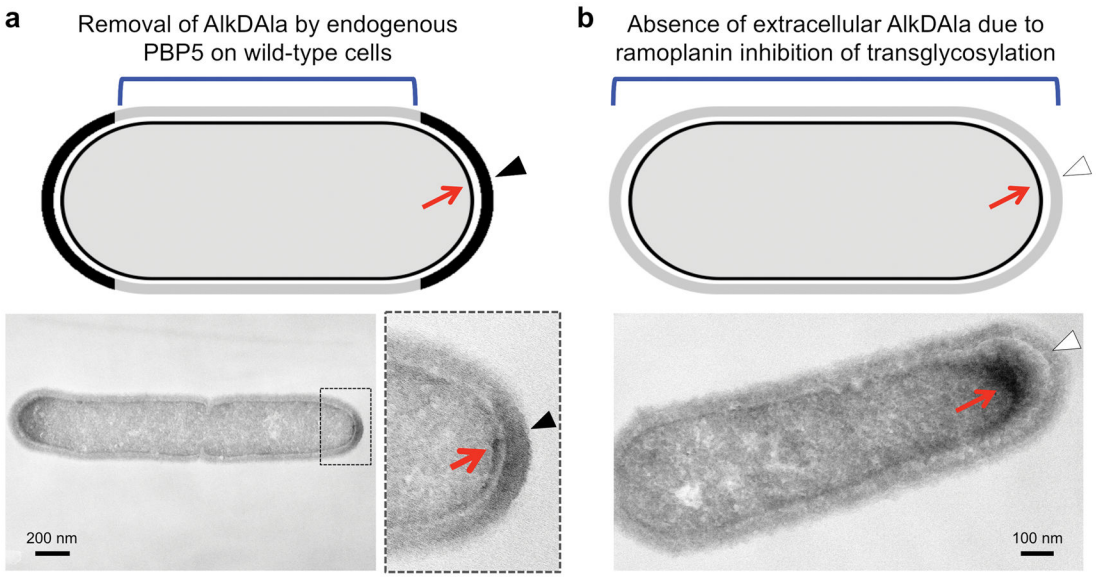

Figure 6. Click-EM imaging of wild type and ramoplanin-treated *L. monocytogenes*

(**a**) Schematic depicting the expected staining pattern of AlkDAla-labeled wild type *L. monocytogenes* cells (top). AlkDAla is removed along the cell length by the endogenous PBP5, resulting in polar staining of extracellular PG (black arrowheads); labeled intracellular precursors are observed as a continuous contour on the cytoplasmic face of the cell membrane (red arrows). (**b**) Schematic depicting the expected staining pattern of ramplanin-treated wild type *L. monocytogenes* cells (top). Ramoplanin inhibits the transglycosylation step of PG synthesis and prevents incorporation of AlkDAla-containing disaccharide-pentapeptide monomers into the extracellular PG mesh. Labeling of extracellular PG is not detected on drug-treated cells (white arrowheads), while labeled intracellular precursors remained visible (red arrows).